

Multi-fingered Robot Hand Compliant Manipulation based on Vision-based Demonstration and Adaptive Force Control

Chao Zeng, *Member, IEEE*, Shuang Li, *Student Member, IEEE*, Zhaopeng Chen, Chenguang Yang, *Senior Member, IEEE*, Fuchun Sun, *Fellow, IEEE*, and Jianwei Zhang, *Member, IEEE*

Abstract—Multi-fingered hand dexterous manipulation is quite challenging in the domain of robotics. One remaining issue is how to achieve compliant behaviours. In this work, we propose a human-in-the-loop learning-control approach for acquiring compliant grasping and manipulation skills of a multi-finger robot hand. This approach takes the depth image of the human hand as input and generates the desired force commands for the robot. The markerless vision-based teleoperation system is used for the task demonstration, and an end-to-end neural network model (i.e., TeachNet) is trained to map the pose of the human hand to the joint angles of the robot hand in real-time. To endow the robot hand with compliant human-like behaviours, an adaptive force control strategy is designed to predict the desired force control commands based on the pose difference between the robot hand and the human hand during the demonstration. The force controller is derived from a computational model of the biomimetic control strategy in human motor learning, which allows adapting the control variables (impedance and feedforward force) online during the execution of the reference joint angles. The simultaneous adaptation of the impedance and feedforward profiles enables the robot to interact with the environment compliantly. Our approach has been verified in both simulation and real-world task scenarios based on a multi-fingered robot hand, i.e., the Shadow Hand, and has shown more reliable performances than the current widely-used position control mode for obtaining compliant grasping and manipulation behaviours.

Index Terms—Robot compliant manipulation; Adaptive impedance/force control; Neural network model; Vision-based teleoperation.

I. INTRODUCTION

It is a major goal in robotic manipulation research to augment robots with human-like dexterous and compliant behaviour for many tasks in daily life [1]–[4]. In recent years numerous attempts have been published towards this goal, but some issues are still not fully addressed yet, especially for grasping and manipulation with a multi-finger robot

This work was supported jointly by the German Research Foundation (DFG) and the National Science Foundation of China (NSFC) in project DEXMAN under grant No.410916101, and the project in Cross Modal Learning TRR-169. C. Zeng and S. Li contributed equally to the work. (*Corresponding author: Chao Zeng*)

C. Zeng, S. Li, and J. Zhang are with TAMS group (Technical Aspects of Multimodal Systems), Department of Informatics, Universität Hamburg, Germany.

Z. Chen is with Agile Robots AG, München, Germany

C. Yang is with Bristol Robotics Laboratory, University of the West of England, UK.

F. Sun is with Department of Computer Science and Technology, Tsinghua University, Beijing, China.

Corresponding email: chaozeng@ieee.org

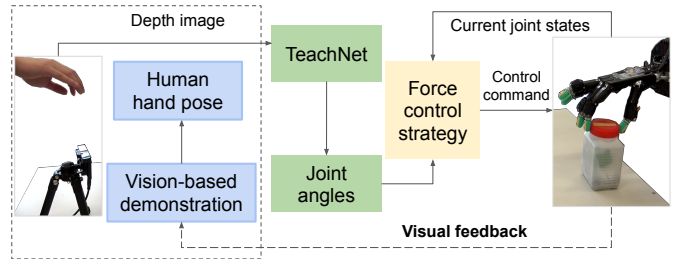


Fig. 1: The pipeline of the proposed human-in-the-loop approach for robot compliant manipulation. The human demonstrator guides the robot hand to complete a task through the vision-based teleoperation. A camera is used to track the hand pose during the demonstration. The neural network model TeachNet is used to map the human hand pose to the robot hand joint angles. Subsequently, a force control strategy is designed to generate the desired force commands for the robot hand during the demonstration loop.

hand [5]–[7]. Most of the state-of-the-art works in robotic grasping mainly focused on object recognition or grasping motion planning (see, e.g., [8]–[10]), and the robotic hand was controlled in a binary way—closing fingers to grasp the object. The task dynamics during the grasping process were often neglected. This kind of control strategy is not suitable for a complex task in which a fine-tuned grasp posture and compliance fingers motions are needed. Yet, we humans can spontaneously adapt our hand pose and force to interact with environments in a compliant manner during daily manipulation tasks. Consequently, if we would like to endow a robot with human-like skills, one promising solution is therefore to develop adaptive control strategies that allow the robot to compliantly deal with physical and dynamical interactions with the environment [11]–[15].

Teleoperation is considered as an efficient way for the robot to imitate manipulation behaviours from humans [16], [17]. Recently, markerless vision-based teleoperation offers several advantages for anthropomorphic robots such as a low cost and no obstructions due to measurement devices. In a typical teleoperation system, the human demonstrator’s behaviours are captured through a motion tracking device and then mapped into the robot’s motion policies in the Cartesian space or joint space. In this case, the robot is often required to be controlled under the position control mode. As a matter of fact, several studies have revealed that (impedance-based) force control strategies could obtain good performances for robot compliant manipulation (see, e.g., [18]–[21]). Thus, it is reasonable to

integrate an adaptive force control strategy into a vision-based teleoperation system such that we can bring their advantages together for the manipulation of the multi-fingered robotic hand.

In this work, we propose a human-in-the-loop learning-control approach combining a vision-based teleoperation system with adaptive force control, allowing us to take an image as the input and output the desired force commands for the robot hand. The pipeline of the proposed approach is shown in Fig. 1. For the learning part, we design an end-to-end neural network model (TeachNet) to learn the mapping relation between the human hand pose and the joint angles of the Shadow robot hand. At run time, a camera is used to collect a depth image of the hand, and the TeachNet estimates the desired robot joint angles based on the image. To deal with task dynamics during hand grasping and manipulation, we develop an adaptive force control strategy which can predict the next-step desired control commands based on the desired joint angles and the robot current states. Our force controller is derived from the computation model inspired by the human motor learning principles. The control variables in the controller, i.e., impedance and feedforward terms are simultaneously adapted online and combined to generate the force/torque commands which are subsequently sent to the robot hand in the joint space.

Some initial results of this work have been partly reported in our conference papers accepted by IEEE/RSJ International Conference on Intelligent Robots and Systems (IROS) 2021 [22], and by International Conference on Robotics and Automation (ICRA) 2019 [23]. This work explains the proposed approach in more details about both the vision-based demonstration part and the force control strategy. Furthermore, it is successfully implemented in real-world experiments based on a tendon-driven multi-fingered robot hand.

To summarize, the novelties and contributions are highlighted as below

i) A human-in-the-loop markerless vision-based teleoperation system is proposed for robot hand demonstration. An end-to-end neural network model is correspondingly trained for the pose mapping from the human hand to the robot hand.

ii) An impedance-based force control strategy is proposed and integrated into teleoperation system. It enables to generate the desired force control commands based on the current hand pose difference. Our approach can realize more compliant manipulation behaviours than the widely-used position control mode in this topic.

and iii) Our approach is verified both in simulation and real-world environments on several different types of tasks. It is worthy mention that, to the best of our knowledge, very few works have reported the implementation of adaptive force control to a tendon-driven multi-fingered robot hand like the Shadow Hand used here, for learning of compliant skills.

II. RELATED WORK

A. Markerless vision-based teleoperation

Vision-based teleoperation systems have been widely used for robots learning skills from human demonstrations [5],

[16], [24]. Typically, a human demonstrator and a robot together constitute a human-in-the-loop leader-follower system, in which a motion-tracking device (such as LeapMotion and Kinect) is usually utilized to capture the human demonstrator's movements. Then, the demonstrated motion is further mapped to the robot's workspace to enable the imitation of the human behaviours. Compared with wearable device-based teleoperation techniques (such as a data glove or a marker-based tracking system) [25]–[27], markerless vision-based approaches allow for natural and unrestricted demonstrations due to non-invasiveness.

A core issue in this end-to-end teleoperation system is how to map the human hand pose to the robot hand pose. Since deep learning (DL) techniques offer the advantages of learning highly non-linear relations, several DL-based hand pose estimation methods have been proposed recently. In [28], [29], the authors proposed to track keypoints of the human hand, then use retargeting methods (e.g., inverse kinematics) to control the robot. Nevertheless, they usually suffer the time cost of the retargeting post-processing. Thus, our previous work [23] proposed a neural network model that permits end-to-end efficient mapping from the 2D depth image representing the human hand pose to the robot hand joint angles. This work aims to extend [23] to further enable the mapping from the image to the desired force commands, which achieve better performances, as observed in the experiments in Section V.

B. Grasping and manipulation based on force/torque control

An impedance-model based force controller has been used in robotic manipulator control for a number of physical interaction tasks (see, e.g., [30]). However, so far it has not been fully investigated yet to control multifingered robot hands for grasping and manipulation tasks. Recent studies illustrate that force control strategies increase the grasping stability and robustness [31], [32], achieve a good grasp stability [33], object handover [34], in-hand manipulation [35], and arm-hand coordination adaptation for contact-rich tasks [36].

In [37], an object-level impedance controller has been developed and shown the effectiveness and robustness for robot grasping. Li *et al.* improved the controller by decomposing the impedance into two parts: one for stable grasping and another for manipulation. Furthermore, the desired impedance is estimated using supervised learning based on the data collected from the human demonstration in advance [38]. Pfanne *et al.* proposed an object-level impedance controller based on in-hand localization, which improved the ability to avoid contact slippage through adjusting the desired grasp configurations [35]. Garate *et al.* proposed to regulate the control of the grasping impedance (stiffness) by regulating both the robot hand pose and the finger joint stiffness. By adapting the magnitude and the geometry of the grasp stiffness, the desired stiffness profile could be achieved to adapt the hand configuration for stable grasping [39].

However, these force controllers may not be suitable for our use in a vision-based teleoperation system, where the controller needs to dynamically respond to the changes of the human hand pose to predict the desired force commands.

Consequently, the contribution of this work is to explore the regulation of the impedance (stiffness) and the feedforward term online during the process of robot grasping or manipulation, which cannot be learned in advance or through exploration.

C. Biomimetic compliant control for robot manipulation

Recently, the biomimetic control strategy inspired by the findings of human motor learning in the muscle space has been developed and proved to be an effective way for robot compliant manipulation [40]. It has been discovered in neuroscience that humans can simultaneously adapt the arm impedance and feedforward force to minimize motion error and interaction force with external environments, under a certain set of constraints [41]. Based on this principle, a biomimetic force controller was first proposed in [42] which allowed the robots to deal with both stable and unstable interactions through the adaptation of the impedance and feedforward term in the force controller. Li *et al.* further improved this controller and implemented it to deal with several physical interaction tasks such as cutting and drilling by a redundant robot manipulator [18]. However, until this work the biomimetic control strategy has not been utilized for a dexterous robot hand with multiple DOFs. Another contribution of this work is to extend the biomimetic force controller to enable compliant grasping and manipulation from human hand teleoperation.

D. Force control on tendon-driven robot hands

To apply a force controller to a tendon-driven robot hand is usually more challenging than to a motor-driven robot hand in the joint space, due to the highly nonlinear characteristics. So far, very few results have been reported in the literature. Typically, Deshpande *et al.* developed a force-optimized joint controller [43] for the tendon-driven robot ACT Hand, and applied it to control one joint (i.e., the MCP joint) of that hand in several tracking experiments. In [32] and [34], the authors proposed to utilize force control to increase grasping stability of the tendon-driven Shadow Hand. If there are perturbations applied to the grasped object, for example, the joint control force could be increased in a straightforward manner, to overcome the perturbations. In this work, we demonstrate that force control is capable of dealing with more complex manipulation tasks beyond grasping, and to enable learning of compliant actions, thanks to the proposed adaptation mechanism mentioned above.

III. ESTIMATION OF ROBOT JOINT ANGLES FROM VISION-BASED TELEOPERATION

In this section, we will present the principles and architecture of the end-to-end neural network TeachNet and the dataset generation.

A. Teacher-student network (TeachNet)

The goal of this section is to find an accurate model to map the human hand image I_H to the corresponding robotic joint Q . We divide this mapping problem into two phases: the

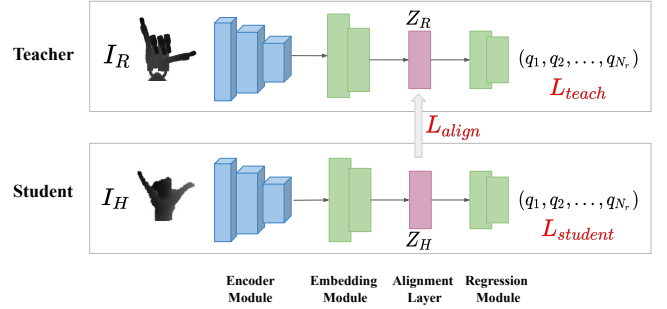


Fig. 2: Overview of TeachNet. TeachNet contains two branches: the teacher branch and the student branch. The input depth images of robot hand I_R and human hands I_H are fed to the corresponding branch that predicts the robot joint angles Q . The student branch is supervised by the joint angle loss $L_{student}$ and the alignment loss L_{align} . The alignment loss aims to exploit the geometrical resemblance between the human hands and the robotic hand.

feature extraction phase f_{feat} and the joint regression phase $f_{regress}$, and formulate:

$$\begin{aligned} f_{feat} : I_H \in \mathbb{R}^2 &\rightarrow Z_{pose} \\ f_{regress} : Z_{pose} &\rightarrow Q \in \mathbb{R}^{N_r \times 1} \end{aligned} \quad (1)$$

Where Z_{pose} means the latent feature in the pose space, and N_r is the number of DOFs.

Assume that we have a pairwise robotic hand and human hand, while the robotic hand performs just the same as the human hand. Even though the robot hand is anthropomorphic, the length of the fingers, the joint ranges, and the structure of the thumb is quite different. The end-to-end method to solve this problem is quite challenging because the human hand and shadow hand basically come from different domains, thus it could be difficult for f_{feat} to learn a meaningful latent feature Z_{pose} . On the contrary, the mapping from I_R to joint target Q is more natural since it is exactly a well-defined hand pose estimation problem. Intuitively, we believe that the latent pose features Z_{pose} of a paired human-robot image should be encouraged to be consistent because they manifest the same hand posture and will be eventually mapped to the same joint target. Based on the above considerations, we devise a novel teacher-student network (TeachNet) to tackle the human-in-the-loop vision-based teleoperation (1) in an end-to-end fashion.

As illustrated in Fig. 2, TeachNet consists of two branches, the teacher branch, which takes I_R as input, and the student branch, which learns robot joint angles from human hand images I_H . The architecture of each branch contains four components: the encoder module, the embedding module, the alignment layer, and the regression module. The encoder module contains an initial convolution layer with 64 filters, batch normalization (BN), and 3×3 max-pooling, following three residual modules, each with a stride of 3×3 , and with 128, 256, 512 filters. By the embedding module, a 128 embedding feature is generated by one fully-connected (FC) layer with batch normalization followed by a Rectified Linear Unit (ReLU) activation and the other FC layer. The regression module follows at the end of the encoder-decoder structure, outputting a joint vector representing the joint angles Θ of

the Shadow hand. Each branch is supervised with a mean squared error (MSE) loss L_{ang} and the physical loss L_{phy} which enforces the physical constraints and joint limits.

$$L_{ang}(Q) = \|Q - Q_g\|^2 \quad (2)$$

where Q_g is the groundtruth joint angles.

$$L_{phy}(Q) = \sum_i [\max(0, (Q_i - Q_{max})) + \max(0, (Q_{min} - Q_i))] \quad (3)$$

The alignment layer is constituted by two latent features Z_R and Z_H . An alignment loss L_{align} between Z_H and Z_R is designed to explore the kinematic similarity between human hands and the robotic hand. Therefore, L_{align} supervises the student branch to be consistent with the teacher branch.

$$L_{align} = \|Z_H - Z_R\|_2 \quad (4)$$

The overall training objective for each branch is:

$$L_{teach}(Q) = L_{ang} + \beta * L_{phy} \quad (5)$$

$$L_{student}(Q) = L_{ang} + \alpha * L_{align} + \beta * L_{phy} \quad (6)$$

where α, β are scaling factors.

The input images are extracted from the raw depth image as a fixed-size cube around the hand relied on the groundtruth keypoints then resized to 100×100 . At the training time, we use minibatch stochastic gradient descent to update θ_{teach} , $\theta_{student}$ for each branch, and apply Adam optimizer with a learning rate of 0.001, scaling parameters $\beta = 1$, $\alpha = 0.1$, training epoch $E = 200$. The learning rate is decayed by 0.5 every 80 epochs. At inference time, we remove the pixels far away from the hand area and extract the hand area after an erosion followed by dilation. And only the student branch is required for reference, thereupon, TeachNet takes an image of a human hand as input and then outputs the estimated joint angles Q of the robot hand.

B. Dataset Generation

To train the TeachNet, which finds out the kinematic retargeting between the human hand and the robot hand, highly depends on a vast dataset with human-robot pairings. Instead of costly collecting robot data on the real robot, we propose to generate human-robot pairing by utilizing an existing dataset BigHand2.2M Dataset [44] with annotated depth images of the human hands, then operating the robot and collecting corresponding joint angles and images in simulation.

BigHand2.2M dataset contains 2.2 million depth maps with precisely annotated 3D joint positions with respect to the camera coordinate. There are 21 keypoints for every hand, including one wrist position and four keypoint positions of each finger. The four keypoints are the TIP (fingertip), MCP (metacarpal), DIP (distal interphalangeal), and PIP (proximal interphalangeal). On the other hand, the fingers of the robot hand also have four joints, i.e., the distal, middle, proximal, and metacarpal joint, but the little finger and the thumb are equipped with an extra joint for supporting the objects.

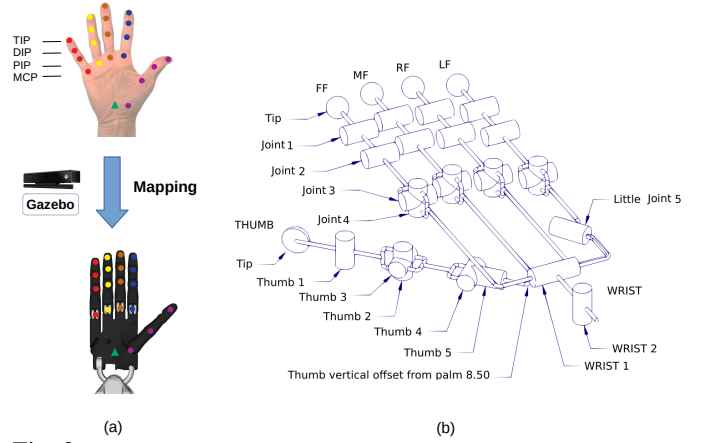


Fig. 3: (a) Keypoints distribution of the human hand in BigHand2.2 dataset and the Shadow hand with BioTac sensors. (b) The kinematic chain of the Shadow robot hand. FF, MF, RF, LF refer to first finger, middle finger, ring finger and little finger.

Moreover, the wrist joint has another two DOFs. Unlike human fingers, especially the thumb are compliant in manipulation, four primary fingers of the robot have the same length, and joint ranges are quite limited. The keypoints distribution of the hand models and the kinematic chain of the robot hand is shown in Fig. 3.

To get the corresponding robot hand in the same poses, we propose an optimized retargeting method integrating position mapping, orientation mapping, and properly considering possible self-collisions by BioIK inverse kinematic solver [45]. The bio-ik solver takes a weighted set of these mapping goals and converges to an optimal joint configuration. Position goals try to match the positions of five robot fingertips and five PIP links with the corresponding human hand positions. The direction goals are applied to five PIP links and DIP link of thumb and tend to match these link axes with the directions of corresponding human phalangeal links. In case BioIK calculates a self-collision solution, we further define a cost function to penalize if the distance between two links is less than the minimum contact radius.

After obtaining the mapping joint angles, the robot moves in Gazebo, then recording current robot joint angles and images. To this end, a training dataset, that contains 400K pairs of simulated robot and human hand depth images and corresponding robot joint angles, was efficiently collected.

IV. FORCE CONTROL STRATEGY

A. Controller formulation

We consider that each finger of the robot hand is controlled independently using impedance-based force controller in the joint space. The control input τ_c is composed of three components [18]

$$\tau_c = \tau_0 - u - v, \quad (7)$$

where u and v are the impedance and feedforward, respectively, and τ_0 is determined by

$$\tau_0 = M\ddot{q}_e + C\dot{q}_e + G - \Gamma\varepsilon, \quad (8)$$

TABLE I: Integration of the vision-based demonstration and the force control strategy for robot compliant manipulation

I TeachNet model training	
Input	
The depth images of the human hand I_H ;	
The depth images of the robot hand I_R ;	
Training epoch N ;	
Output	
The trained TeachNet model;	
Begin	
Initialize the parameters $\theta_{teach}, \theta_{student}$;	
While <i>epoch not end</i> do	
Compute training objective L_{teach} in teacher branch;	
Compute training objective L_{stud} in student branch;	
Compute adapted parameters with gradient descent;	
Update θ_{teach} and $\theta_{student}$ respectively.	
End	
End	
II Online generation of the force control command	
Input	
The learned optimal TeachNet model f_m ;	
The constant coefficients: $\Theta_k, \Theta_d, \Theta_v$, and π ;	
The Gaussian basis g .	
Begin	
Initialize the parameters θ_k, θ_d , and θ_v ;	
While <i>online teleoperation</i> do	
Sense an image of the human hand pose I_h ;	
Calculate the desired pose of the robot hand;	
Get the robot current states;	
Calculate the sliding error ε ;	
Update parameters θ_k, θ_d and θ_v ;	
Generate the desired force control commands τ_c	
Send the effort commands to the robot joint space.	
End	
End	

with a symmetric positive-definite matrix Γ with minimal eigenvalue, and ε is the sliding error which will be defined later. M , C and G denote the inertia, the Coriolis and centrifugal forces, and gravitational force, respectively. \dot{q}_e is an auxiliary variable, given by,

$$\dot{q}_e = \dot{q}_d - \pi e, \quad \ddot{q}_e = \ddot{q}_d - \pi \dot{e} \quad (9)$$

and

$$e = q - q_d, \quad \dot{e} = \dot{q} - \dot{q}_d \quad (10)$$

where $e \in R^{N_r \times 1}$ and $\dot{e} \in R^{N_r \times 1}$ represent the errors of the joint angles and velocities between the current ($q \in R^{N_r \times 1}$ and $\dot{q} \in R^{N_r \times 1}$) and desired ($q_d \in R^{N_r \times 1}$ and $\dot{q}_d \in R^{N_r \times 1}$) ones.

The impedance is determined using a PD form,

$$u = K_s e + K_d \dot{e}, \quad (11)$$

with

$$\begin{cases} K_s = \text{diag}\{K_{s,1}, K_{s,2}, \dots, K_{s,N_r}\} \\ K_d = \text{diag}\{K_{d,1}, K_{d,2}, \dots, K_{d,N_r}\} \\ v = \{v_1, v_2, \dots, v_{N_r}\} \end{cases}, \quad (12)$$

where $K_s \in R^{N_r \times N_r}$ and $K_d \in R^{N_r \times N_r}$ denote the stiffness and damping matrix, respectively.

TABLE II: Explanation of the cost functions

	Notation	Implication
Sec. III	L_{ang}	MSE loss for training the NN model
	L_{align}	guarantee the consistency between two branches
	L_{phys}	handle the physical constraints and joint limits
Sec. IV	L_e	minimize the tracking errors of joint angles
	L_c	deal with the interaction dynamics

Then, we parametrize all the compliant profiles (i.e., K_s , K_d , and v) as [46],

$$K_{s,i} = \theta_{k,i}^T g, \quad K_{d,i} = \theta_{d,i}^T g, \quad v_i = \theta_{v,i}^T g, \quad (13)$$

where $\theta_k \in R^{N_r \times N}$, $\theta_d \in R^{N_r \times N}$, and $\theta_v \in R^{N_r \times N}$ denote the parameters corresponding to the compliant profiles, i.e., stiffness, damping and feedforward force, respectively. And $g \in R^{N \times 1}$ is the Gaussian basis, and it is determined by,

$$[g]_n = \frac{\omega_n(s)}{\sum_{n=1}^N \omega_n(s)}, \quad (14)$$

with

$$\omega_n(s) = \exp(-0.5h_n(s - c_n)^2), \quad (15)$$

where s is the variable that can be calculated by $\dot{s} = -s$. c_n and h_n are the centers and widths of the basis, and N is the total number of the Gaussian models.

B. Cost definition

The parameters θ_k , θ_d and θ_v need to be adapted at each time step based on the desired and current robot states, to generate the desired control force. To do so, we consider the following costs.

First, for the minimization of the tracking error, we consider the following cost which is often used in robot control domain,

$$L_e = \frac{1}{2} \varepsilon^T M \varepsilon, \quad (16)$$

where ε is a sliding error, determined by $\varepsilon = \dot{e} + \pi e$, and π is a positive constant.

Then, we consider the the following cost to deal with the the interaction dynamics [42],

$$L_c = \frac{1}{2} \tilde{\Phi}^T \Theta^{-1} \tilde{\Phi}, \quad (17)$$

where

$$\tilde{\Phi} = \Phi - \Phi^* = [\tilde{\theta}_k^T, \tilde{\theta}_d^T, \tilde{\theta}_v^T]^T, \quad (18)$$

with

$$\Phi = [\bar{\theta}_k^T, \bar{\theta}_d^T, \bar{\theta}_v^T]^T, \quad (19)$$

and

$$\Phi^*(t) = [\bar{\theta}_k^{*T}, \bar{\theta}_d^{*T}, \bar{\theta}_v^{*T}]^T, \quad (20)$$

where $\theta_k^*(t)$, $\theta_d^*(t)$, and $\theta_v^*(t)$ denote the desired parameters, respectively corresponding to the desired stiffness, damping and feedforward force. $(\bar{\cdot})$ denotes the row average vectors

of the corresponding parameters. The matrix Θ is determined according to,

$$\Theta = \text{diag}(\Theta_k \otimes \mathbf{I}, \Theta_d \otimes \mathbf{I}, \Theta_v \otimes \mathbf{I}), \quad (21)$$

where $\Theta_k \in R^{N_r \times N_r}$, $\Theta_d \in R^{N_r \times N_r}$ and $\Theta_v \in R^{N_r \times N_r}$ are symmetric positive-definite matrices which are manually set in the experiments. \mathbf{I} is an identity matrix.

C. Adaptation law

The derivation of the adaptation law is similar to the process in our previous work [46]. The updating goal is to minimize the overall cost, i.e., $\min \|L_c + L_e\|$. First, we have τ_{ext} considering the external force

$$\tau_{ext} = K_s^* e + K_d^* \dot{e} + v^*. \quad (22)$$

where K_s^* , K_d^* , and v^* are the desired stiffness, damping, and feedforward force that compensate for the interaction dynamics [18].

Combining (8) and the following robot dynamics

$$M\ddot{q} + C\dot{q} + G = \tau_c + \tau_{ext}, \quad (23)$$

We can obtain

$$M(\ddot{q} - \ddot{q}_e) + C(\dot{q} - \dot{q}_e) = -u - v + \tau_{ext} - \Gamma\varepsilon. \quad (24)$$

Recalling (9) and (10), we get

$$M\dot{\varepsilon} + C\varepsilon = -u - v + \tau_{ext} - \Gamma\varepsilon. \quad (25)$$

Combining with (22), it yields

$$M\dot{\varepsilon} + C\varepsilon = -\tilde{K}_s e - \tilde{K}_d \dot{e} - \tilde{v} - \Gamma\varepsilon. \quad (26)$$

The time derivative of L_c ,

$$\begin{aligned} \dot{L}_c &= \tilde{\Phi}^T \Theta^{-1} \dot{\tilde{\Phi}} \\ &\approx \tilde{\theta}_k^T \Theta_k^{-1} \dot{\tilde{\theta}}_k + \tilde{\theta}_d^T \Theta_d^{-1} \dot{\tilde{\theta}}_d + \tilde{\theta}_v^T \Theta_v^{-1} \dot{\tilde{\theta}}_v. \end{aligned} \quad (27)$$

And the time derivative of L_e ,

$$\begin{aligned} \dot{L}_e &= \varepsilon^T M\dot{\varepsilon} + \frac{1}{2} \varepsilon^T \dot{M}\varepsilon = \varepsilon^T (M\dot{\varepsilon} + C\varepsilon) \\ &= -[\varepsilon^T (\tilde{K}_s e + \tilde{K}_d \dot{e} + \tilde{v})] - \varepsilon^T \Gamma\varepsilon, \end{aligned} \quad (28)$$

with

$$\tilde{K}_s = \text{diag}\{\tilde{\theta}_k^T g\}, \tilde{K}_d = \text{diag}\{\tilde{\theta}_d^T g\}, \tilde{v} = \tilde{\theta}_v^T g. \quad (29)$$

Subsequently, the time derivative of the overall cost is

$$\begin{aligned} \dot{L}_{all} &= \dot{L}_c + \dot{L}_e \\ &= \tilde{\theta}_k^T \Theta_k^{-1} \dot{\tilde{\theta}}_k - \varepsilon^T \text{diag}\{\tilde{\theta}_k^T g\} e \\ &\quad + \tilde{\theta}_d^T \Theta_d^{-1} \dot{\tilde{\theta}}_d - \varepsilon^T \text{diag}\{\tilde{\theta}_d^T g\} \dot{e} \\ &\quad + \tilde{\theta}_v^T \Theta_v^{-1} \dot{\tilde{\theta}}_v - \varepsilon^T (\tilde{\theta}_v^T g) - \varepsilon^T \Gamma\varepsilon. \end{aligned} \quad (30)$$

Then, we need to adapt the the stiffness, damping and feedforward force for the minimization of the above cost,

$$\begin{aligned} \tilde{\theta}_k^T \Theta_k^{-1} \dot{\tilde{\theta}}_k &= \varepsilon^T \text{diag}\{\tilde{\theta}_k^T g\} e, \\ \tilde{\theta}_d^T \Theta_d^{-1} \dot{\tilde{\theta}}_d &= \varepsilon^T \text{diag}\{\tilde{\theta}_d^T g\} \dot{e}. \end{aligned} \quad (31)$$

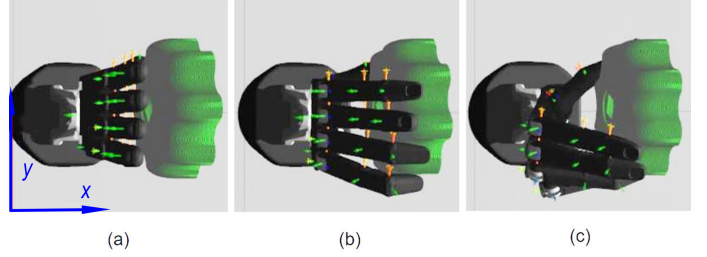


Fig. 4: The turning-a-cap task in simulation. (a), (b) and (c) denote the initial, middle and final configurations.

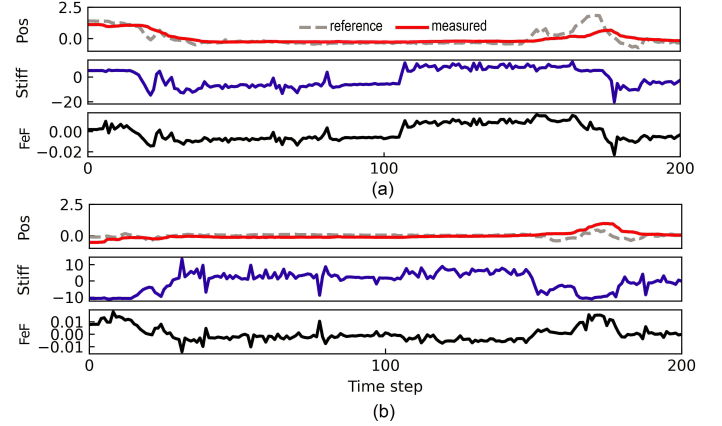


Fig. 5: The online learned compliant profiles including stiffness (stiff.) and feedforward (FeF) force along the execution of the joint angles in the turning-a-cap task. All the profiles are reduced to the 2D space using PCA, the first and second components shown in (a) and (b), respectively. The reference and measured curves mean the joint angles estimated from the TeachNet and collected from the robot hand, respectively.

$$\tilde{\theta}_v^T \Theta_v^{-1} \dot{\tilde{\theta}}_v = \varepsilon^T \text{diag}\{\tilde{\theta}_v^T g\}.$$

Here, we consider the time-invariant environment. Then, we have

$$\dot{\tilde{\theta}}_k = \dot{\theta}_k - \dot{\theta}_k^* \approx \dot{\theta}_k. \quad (32)$$

For the n_r -th ($n_r \in [0, \dots, N_r]$) DOF, we utilize the following adaptation way to satisfy above equations,

$$\begin{aligned} \dot{\tilde{\theta}}_{k,n_r}^T &= \Theta_{k,n_r} \varepsilon_{n_r} e_{n_r} g, \\ \dot{\tilde{\theta}}_{d,n_r}^T &= \Theta_{d,n_r} \varepsilon_{n_r} \dot{e}_{n_r} g, \\ \dot{\tilde{\theta}}_{v,n_r}^T &= \Theta_{v,n_r} \varepsilon_{n_r} g. \end{aligned} \quad (33)$$

Table I summarizes the procedure of the integration of the vision-based demonstration and the force control strategy. Table II summarizes the notations and implications of the cost functions used in this work.

V. SIMULATION EXPERIMENTS

A. Simulation setup

A real-sim setup is established for the simulation experiments. In the experiments, the human operator performs different hand poses to guide the simulated robot hand to complete the tasks with visual feedback. A camera (Intel RealSense SR300) is used to capture the depth images of

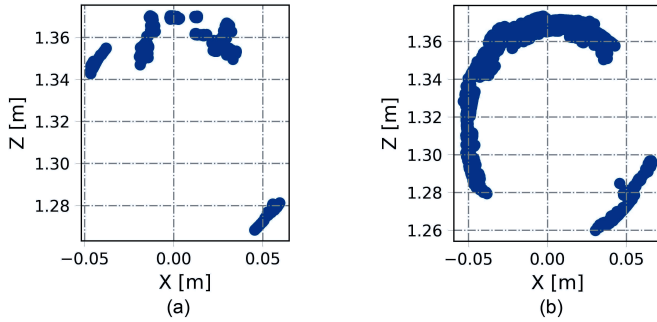


Fig. 6: The positions of the contact points in the $x - z$ plane during the turning process, under the (a) position control and (b) adaptive force control modes, respectively.

TABLE III: The measured contact force values during the touching phase.

Force [N]	Adaptive force	Position mode
Average force	0.41	1.781
Max force	2.452	7.388

the human hand, based on which the desired robot hand pose can be estimated via the TeachNet model. The virtual Shadow Motor Hand in the Gazebo simulator with the ODE engine is utilized for our experiments, based on the ROS package¹ provided by the Shadow Robot Company. In our usage, the Shadow robot hand is torque-controlled under the TEACH mode. The simulation environment is run on the Ubuntu 18.04 system with a CPU Intel Core i5-8500 and a NVIDIA 1050 Ti GPU. The average updating time at each time is 0.036 s.

B. Simulation results

To verify whether the proposed adaptive force control could yield more compliant performances, we compare the proposed force control with position control on two tasks i.e., turning-a-cap and touching-a-mouse.

Under the position control mode, the position commands from TeachNet model are directly used to control the robot hand. Notely, while virtual environments are dominated by physics (e.g. object weights and surface frictions) the absence of the force feedback makes the tasks rather challenging [47], as even slight inaccuracies on joint angles from TeachNet may result in failure interactions. The details of the two tasks are presented as follows.

Turning-a-cap: In this task, the robot hand is teleoperated by the human demonstrator to turn a cap using five fingers. The frame of the cap is fixed in the Gazebo world, and the cap can be rotated in the $x - z$ plane. In a real-world task like turning a cap, humans need to adapt the motion of both arm and hand coordinately to complete this task. More importantly, the rotation of the wrist joint plays a key role during the turning process. In our teleoperation system, however, the fixed base and wrist of the Shadow hand make this task more challenging than usual. The robot hand is guided to make contact with the cap using a proper configuration and then to adapt the

movements of all the fingers to turn the cap. We observe that the fingers can move coordinately and cooperate well with each other to complete the task using the proposed force control strategy (see Fig. 4 as an example). Then we analyse the compliant profiles including the stiffness and feedforward force learned online with the execution of the task. For better illustration, we reduce the stiffness and the feedforward force of all joints to the 2D space using the PCA algorithm. The results visualized in Fig. 5 indicate that the robot hand (the reference curves) can track the human hand (the real curves) with the online adaptation of the stiffness and feedforward force profiles based on the pose difference between the human and the robot hands. Under the direct position control mode, however, the robot hand fails to turn the cap due to the lack of coordination and dexterity. Furthermore, the distribution of the contact points obtained under the adaptive force mode is more caplike (see Fig. 6).

Touching-a-mouse: To further explore the compliance with the adaptive force control, we investigate the performances when the robot hand contacts with a curved surface by touching a mouse, as shown in Fig. 7(a). We mainly focus on achieving stable contacts between the hand and the mouse surface with small contact forces. Namely, we expect that the robot hand is able to touch the surface of the target object in a more human-like manner. To evaluate the impact of the adaptive control strategy, the task is also conducted under two different control strategies: with the proposed adaptive control and the position control mode. Under each condition, the task is repeated ten times. During each test, the contact points and forces are recorded for evaluation of the performances.

Fig. 7 manifests that under the proposed control mode the contact points of each local region are distributed in a more clustered way than that under the position mode, with comparatively low contact forces. Under the position control mode, there are obvious slippery points with larger contact forces, due to the rigid interaction with the mouse of the robot hand. We collect the contact forces from these tests under each control condition, and calculate the maximum and average forces. The results (see Table III) demonstrate significantly lower average as well as maximum forces with our proposed control strategy.

VI. ROBOTIC VALIDATION

A. Hardware setup

We then evaluate our approach on a real-world Shadow Dexterous Hand with five fingers. Since the first link of each finger is replaced by a BioTac tactile sensor which is rigidly mounted onto the second link, the first joint of each finger is thus fixed. This reduces the controllable DOFs from 22 to 17. We deployed the learned model directly on the hardware system, and it generalized across the reality gap. To implement our control strategy, the robot hand is controlled under the effort-control mode, i.e., the TEACH mode. Furthermore, we map the outputs of our force controller to the effort control commands in a linear manner², instead of directly sending the

²For simplicity, we map the torque values to the tendon efforts by multiplying a constant positive factor, which is chosen empirically. Other nonlinear mapping ways may also be feasible.

¹https://github.com/shadow-robot/sr_core

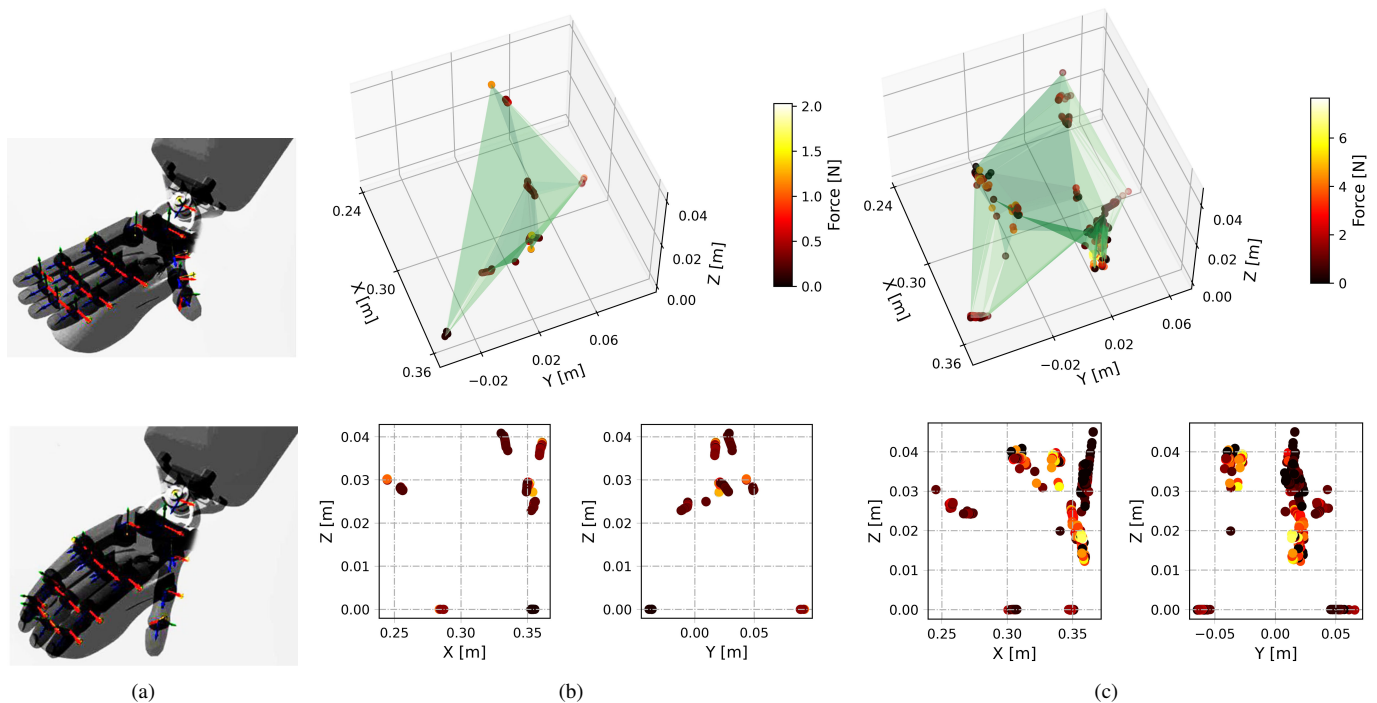


Fig. 7: (a) shows the touching-a-mouse task: before touching (upper row) and after touching (lower row). The distribution of the contact points and the contact force during the touching process under the (b) adaptive force control and (c) position control conditions, respectively. The upper row shows the results in the 3D space, and the lower row shows the corresponding results which are projected to the $x - z$ and $y - z$ planes.

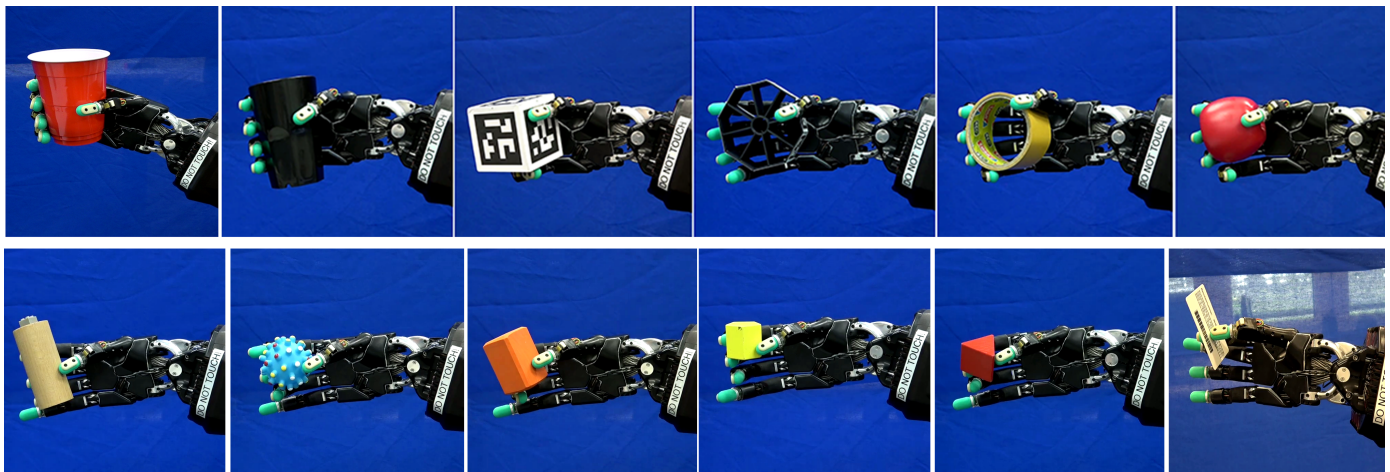


Fig. 8: The results of the grasping tasks. The upper and lower rows show power grasp and tip grasp examples, respectively.

outputs to the joints, due to the tendon-driven mechanism of the Shadow Hand.

B. Experimental results

We start the real-world experiments with grasping tasks (including both tip grasping and power grasping), then test our approach by a pouring-crews-into-a-cup task and a opening-a-bottle-cap task. The experimental video is available here³. The results are reported below.

³<https://youtu.be/8MwA6k7liqU>

Grasping tasks: First, we validate our approach in grasping tasks. As shown in Fig. 8, the robot hand succeeds in grasping objects with different shapes and different sizes, using both power grasp and tip grasp. We compare our approach with the position control mode in grasping a rigid cup, and observe the grasp dynamical process and contact force from the fingertip tactile sensors. As shown in Fig. 9(a)-(b), during each grasp, the human partner holds the cup in a very similar pose, and another subject teleoperates the robot hand to grasp and take over the cup from the human hand. The same subject teleoperates the robot hand under two different modes, using a very similar grasp posture. We repeat the task several times

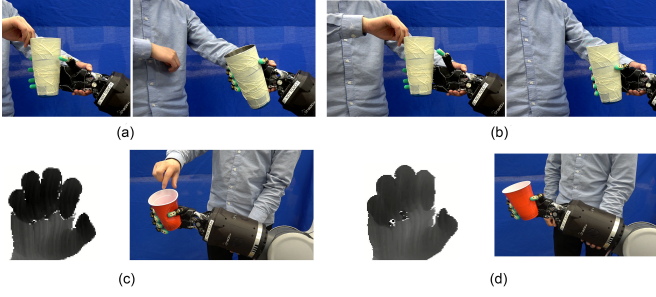


Fig. 9: The illustration of grasping a rigid cup (upper row) and a soft plastic cup (lower row) under (a)(c) position and (b)(d) adaptive force control modes. The left pictures in (c) and (d) are the depth images of the human hand posture.

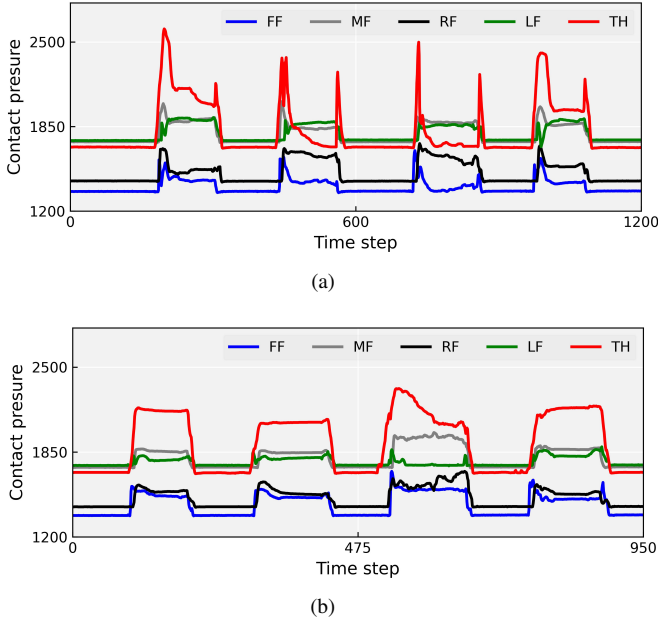


Fig. 10: The measured contact pressure of the five finger tips from the tactile sensors during continuously grasping the rigid cup four times under (a) position mode and (b) adaptive force mode.

and keep the subject using as similar as possible grasp postures for two control modes. The measured contact pressure force is visualized in Fig. 10. It is observed that under the position control mode the robot hand tends to rigidly grasp the cup with larger contact force (especially for the thumb), resulting in an obvious bump at the touching stage of the grasp. Under the adaptive force mode, on the other hand, contact force keeps more steady along the grasping process. We repeat the task several times, similar results are observed in these trials. Then, we also compare the two control modes in grasping a soft plastic cup, as shown in Fig. 9(c)-(d), it turns out that under the position mode the robot hand much more easily gets the cup deformed after contact than the adaptive force control mode.

Pouring-crews-into-a-cup: To illustrate how the force control strategy deals with external disturbances, a pouring task is then performed. The robot hand is teleoperated to hold a cup, the human partner pours a set of screws into the cup, as shown

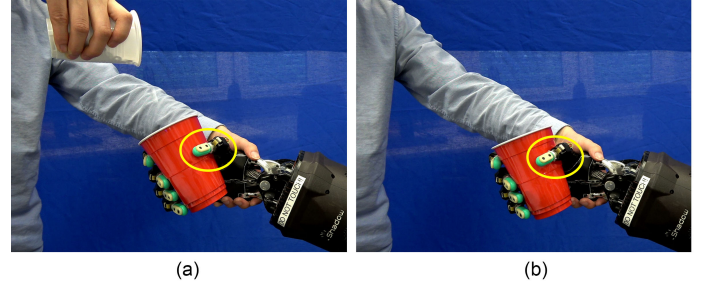


Fig. 11: The screenshots of the pouring-screws-into-a-cup task. (a) and (b) denote before and after pouring, respectively. The wrist joint is held by the human user during the pouring process.

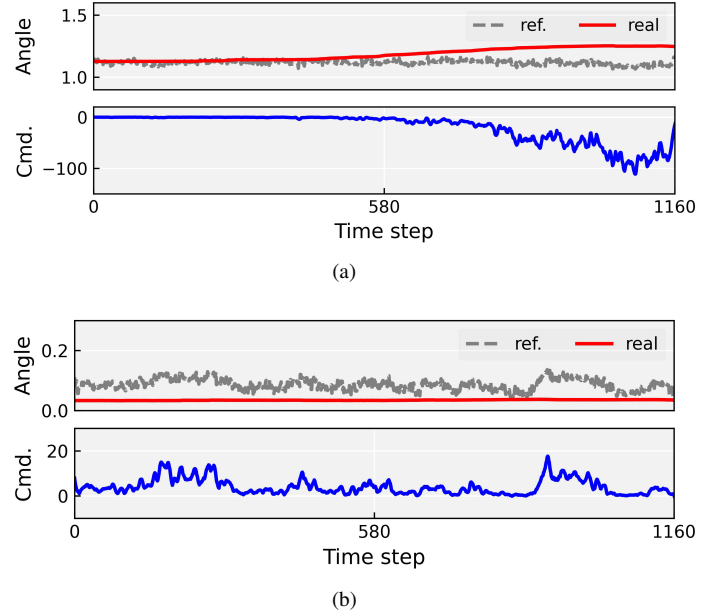


Fig. 12: The measured joint angles (real), the estimated joint angles from TeachNet (ref.), and the joint effort commands of joint (a) THj4 and (b) FFj4 in the pouring-crews-into-a-cup task. Cmd. refers to the commanded efforts.

in Fig. 11. The total weight of the screws is about 0.6 Kg. With the increasing weight, the thumb finger tends to slip slightly. Once the slip happens, the pose error becomes larger, the force controller correspondingly increases the command effort automatically to overcome the slip, and thus to maintain the holding posture stably. Fig. 12(a) visualizes the joint angles (both measured ones from the Shadow robot and estimated ones from TeachNet) and the generated command of the fourth joint of the thumb (i.e., THj4) during the pouring process. The angle of THj4 changes obviously when slip occurs along the vertical direction of the surface of the cup. We observe that the command effort is adapted correspondingly to overcome the slipperiness, in order that the thumb can be stabilized. However, the control effort profiles keep comparatively low if no slipperiness happens, see the profiles of the fourth joint of the first finger (i.e., FFj4) as an example, which is shown in Fig. 12(b). These results suggest that the proposed approach is able to adaptively generate appropriate effort commands to overcome the external

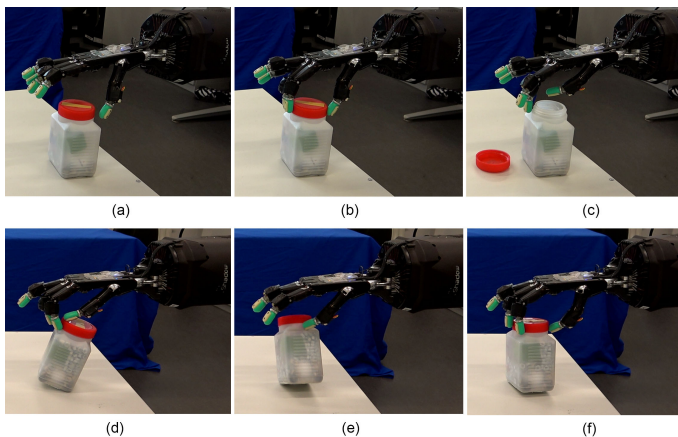


Fig. 13: The screenshots of the opening-a-bottle-cap task. (a), (b) and (c) denote the initial, middle and final configurations under the adaptive force mode, respectively. (d)-(f) show several typical rigid interaction examples under the position mode.

disturbances.

Opening-a-bottle-cap: Finally, we test our approach in a task of opening a bottle cap where requires superior dexterity and compliance of the robot hand. In this task, the PR2 robot arm is fixed, and three fingers (i.e., TH, FF, and MF) of the robot hand are used. To compare the performance of adaptive force control and the position control in this task, the same subject teleoperates the robot under the same task condition. The results demonstrate that the robot can open the bottle cap under the proposed adaptive force control mode [see, Fig. 13(a)-(c)]. On the contrary, we observe that under the position mode the robot hand fingers tend to push the bottle away easily and to interact with the cap quite rigidly [see, Fig. 13(d)-(f)], due to the lack of flexibility and dexterity. Please refer to the experimental video for visualization of the dynamical process.

VII. CONCLUSION AND FUTURE WORK

This work proposes an approach for robotic compliant grasping and manipulation based on the adaptive force control strategy through teleoperation. Our approach takes a depth image of the human hand as the input and predicts the desired force control commands, instead of outputting the motion control policies directly. The proposed strategy online adapts the compliant profiles (impedance and feedforward) in the force controller, based on the pose difference between the human hand and the robot hand step-by-step.

Our approach has been verified in several simulation tasks and real-world robotic tasks. The results show that it can obtain better performances than the state-of-the-art widely-used position control mode for robot compliant grasping and manipulation. It worth mentioning that the robot hand in the simulation environment is motor-driven, but the real-world Shadow hand is tendon-driven. In spite of the different driven mechanisms, our approach can work both in the simulated and real-world hands.

One drawback of our approach lies in relying on the single image modality as input. In future work, we will consider to

improve our approach by exploring multimodal data, especially, by including the tactile feedback. We can estimate the interaction force between the robot hand and its environment from tactile signals collected from the tactile sensors mounted on the tips of the Shadow motor hand. The estimated force information can then be included in the control loop as a feedback variable to increase the interaction dexterity.

Another drawback is that we have to manually set the open parameters which would affect the performances. In the future, one may utilize optimization techniques (e.g., Reinforcement Learning) to optimize the learned the compliant profiles, given the pre-set open parameters. The goal is to further improve the robot's capability of dexterous manipulation after the human-in-the-loop demonstration.

REFERENCES

- [1] A. Billard and D. Kragic, "Trends and challenges in robot manipulation," *Science*, vol. 364, no. 6446, 2019.
- [2] Z. Lu, N. Wang, and C. Yang, "A constrained dmfs framework for robot skills learning and generalization from human demonstrations," *IEEE/ASME Transactions on Mechatronics*, vol. 26, no. 6, pp. 3265–3275, 2021.
- [3] C. Yang, C. Zeng, and J. Zhang, *Robot Learning Human Skills and Intelligent Control Design*. CRC Press, 2021.
- [4] T. Teng, M. Fernandes, M. Gatti, S. Poni, C. Semini, D. Caldwell, and F. Chen, "Whole-body control on non-holonomic mobile manipulation for grapevine winter pruning automation," in *2021 6th IEEE International Conference on Advanced Robotics and Mechatronics (ICARM)*. IEEE, 2021, pp. 37–42.
- [5] F. Ficuciello, A. Migliozi, G. Laudante, P. Falco, and B. Siciliano, "Vision-based grasp learning of an anthropomorphic hand-arm system in a synergy-based control framework," *Science Robotics*, vol. 4, no. 26, 2019.
- [6] K. Z. Zhuang, N. Sommer, V. Mendez, S. Aryan, E. Formento, E. D'Anna, F. Artoni, F. Petrini, G. Granata, G. Cannaviello *et al.*, "Shared human-robot proportional control of a dexterous myoelectric prosthesis," *Nature Machine Intelligence*, vol. 1, no. 9, pp. 400–411, 2019.
- [7] P. Ruppel and J. Zhang, "Learning object manipulation with dexterous hand-arm systems from human demonstration," in *2020 IEEE/RSJ International Conference on Intelligent Robots and Systems (IROS)*. IEEE, 2020, pp. 5417–5424.
- [8] H. Liang, X. Ma, S. Li, M. Görner, S. Tang, B. Fang, F. Sun, and J. Zhang, "Pointnetgpd: Detecting grasp configurations from point sets," in *2019 International Conference on Robotics and Automation (ICRA)*, 2019, pp. 3629–3635.
- [9] J. Mahler, M. Matl, V. Satish, M. Danielczuk, B. DeRose, S. McKinley, and K. Goldberg, "Learning ambidextrous robot grasping policies," *Science Robotics*, vol. 4, no. 26, 2019.
- [10] Q. Lu, M. Van der Merwe, B. Sundaralingam, and T. Hermans, "Multi-fingered grasp planning via inference in deep neural networks: Outperforming sampling by learning differentiable models," *IEEE Robotics & Automation Magazine*, vol. 27, no. 2, pp. 55–65, 2020.
- [11] X. Yu, W. He, H. Li, and J. Sun, "Adaptive fuzzy full-state and output-feedback control for uncertain robots with output constraint," *IEEE Transactions on Systems, Man, and Cybernetics: Systems*, 2020.
- [12] S. Xu, Y. Ou, Z. Wang, J. Duan, and H. Li, "Learning-based kinematic control using position and velocity errors for robot trajectory tracking," *IEEE Transactions on Systems, Man, and Cybernetics: Systems*, 2020.
- [13] W. Dai, L. Zhang, J. Fu, T. Chai, and X. Ma, "Dual-rate adaptive optimal tracking control for dense medium separation process using neural networks," *IEEE Transactions on Neural Networks and Learning Systems*, 2020.
- [14] Z. Yu, Y. Zhang, B. Jiang, C.-Y. Su, J. Fu, Y. Jin, and T. Chai, "Fractional-order adaptive fault-tolerant synchronization tracking control of networked fixed-wing uavs against actuator-sensor faults via intelligent learning mechanism," *IEEE Transactions on Neural Networks and Learning Systems*, 2021.
- [15] J. Fu, Z. Ma, Y. Fu, and T. Chai, "Hybrid adaptive control of nonlinear systems with non-lipschitz nonlinearities," *Systems & Control Letters*, vol. 156, p. 105012, 2021.

- [16] A. Handa, K. Van Wyk, W. Yang, J. Liang, Y.-W. Chao, Q. Wan, S. Birchfield, N. Ratliff, and D. Fox, "Dexpilot: Vision-based teleoperation of dexterous robotic hand-arm system," in *2020 IEEE International Conference on Robotics and Automation (ICRA)*. IEEE, 2020, pp. 9164–9170.
- [17] J. Luo, D. Huang, Y. Li, and C. Yang, "Trajectory online adaption based on human motion prediction for teleoperation," *IEEE Transactions on Automation Science and Engineering*, 2021.
- [18] Y. Li, G. Ganesh, N. Jarrassé, S. Haddadin, A. Albu-Schaeffer, and E. Burdet, "Force, impedance, and trajectory learning for contact tooling and haptic identification," *IEEE Transactions on Robotics*, vol. 34, no. 5, pp. 1170–1182, 2018.
- [19] K. Van Wyk, M. Culleton, J. Falco, and K. Kelly, "Comparative peg-in-hole testing of a force-based manipulation controlled robotic hand," *IEEE Transactions on Robotics*, vol. 34, no. 2, pp. 542–549, 2018.
- [20] J. Duan, Y. Ou, S. Xu, and M. Liu, "Sequential learning unification controller from human demonstrations for robotic compliant manipulation," *Neurocomputing*, vol. 366, pp. 35–45, 2019.
- [21] X. Yu, W. He, Y. Li, C. Xue, J. Li, J. Zou, and C. Yang, "Bayesian estimation of human impedance and motion intention for human-robot collaboration," *IEEE transactions on cybernetics*, 2019.
- [22] C. Zeng, L. Shuang, Y. Jiang, Q. Li, Z. Chen, C. Yang, and J. Zhang, "Learning compliant grasping and manipulation by teleoperation with adaptive force control," in *2021 IEEE/RSJ International Conference on Intelligent Robots and Systems (IROS)*. IEEE, 2021.
- [23] S. Li, X. Ma, H. Liang, M. Görner, P. Ruppel, B. Fang, F. Sun, and J. Zhang, "Vision-based teleoperation of shadow dexterous hand using end-to-end deep neural network," in *2019 International Conference on Robotics and Automation (ICRA)*. IEEE, 2019, pp. 416–422.
- [24] S. Li, J. Jiang, P. Ruppel, H. Liang, X. Ma, N. Hendrich, F. Sun, and J. Zhang, "A mobile robot hand-arm teleoperation system by vision and imu," in *2020 IEEE/RSJ International Conference on Intelligent Robots and Systems (IROS)*. IEEE, 2020, pp. 10 900–10 906.
- [25] I. Cerulo, F. Ficuciello, V. Lippiello, and B. Siciliano, "Teleoperation of the schunk s5fh under-actuated anthropomorphic hand using human hand motion tracking," *Robotics and Autonomous Systems*, vol. 89, pp. 75–84, 2017.
- [26] B. Fang, F. Sun, H. Liu, and C. Liu, "3D human gesture capturing and recognition by the IMMU-based data glove," *Neurocomputing*, vol. 277, pp. 198–207, 2018.
- [27] S. Han, B. Liu, R. Wang, Y. Ye, C. D. Twigg, and K. Kin, "Online optical marker-based hand tracking with deep labels," *ACM Transactions on Graphics (TOG)*, vol. 37, 2018.
- [28] F. Gomez-Donoso, S. Orts-Escolano, and M. Cazorla, "Accurate and efficient 3D hand pose regression for robot hand teleoperation using a monocular RGB camera," *Expert Systems with Applications*, vol. 136, pp. 327–337, 2019.
- [29] D. Antotsiou, G. Garcia-Hernando, and T.-K. Kim, "Task-oriented hand motion retargeting for dexterous manipulation imitation," in *European Conference on Computer Vision (ECCV)*, 2018.
- [30] F. Ficuciello, L. Villani, and B. Siciliano, "Variable impedance control of redundant manipulators for intuitive human–robot physical interaction," *IEEE Transactions on Robotics*, vol. 31, no. 4, pp. 850–863, 2015.
- [31] S. Fan, H. Gu, Y. Zhang, M. Jin, and H. Liu, "Research on adaptive grasping with object pose uncertainty by multi-fingered robot hand," *International Journal of Advanced Robotic Systems*, vol. 15, no. 2, pp. 1–16, 2018.
- [32] Z. Deng, Y. Jonetzko, L. Zhang, and J. Zhang, "Grasping force control of multi-fingered robotic hands through tactile sensing for object stabilization," *Sensors*, vol. 20, no. 4, p. 1050, 2020.
- [33] N. Sommer and A. Billard, "Multi-contact haptic exploration and grasping with tactile sensors," *Robotics and Autonomous Systems*, vol. 85, pp. 48–61, 2016.
- [34] A. G. Eguiluz, I. Rañó, S. A. Coleman, and T. M. McGinnity, "Reliable object handover through tactile force sensing and effort control in the shadow robot hand," in *2017 IEEE International Conference on Robotics and Automation (ICRA)*. IEEE, 2017, pp. 372–377.
- [35] M. Pfanne, M. Chalon, F. Stulp, H. Ritter, and A. Albu-Schäffer, "Object-level impedance control for dexterous in-hand manipulation," *IEEE Robotics and Automation Letters*, vol. 5, no. 2, pp. 2987–2994, 2020.
- [36] J. Gao, Y. Zhou, and T. Asfour, "Learning compliance adaptation in contact-rich manipulation," *arXiv preprint arXiv:2005.00227*, 2020.
- [37] T. Wimbock, C. Ott, and G. Hirzinger, "Analysis and experimental evaluation of the intrinsically passive controller (ipc) for multifingered hands," in *2008 IEEE International Conference on Robotics and Automation (ICRA)*. IEEE, 2008, pp. 278–284.
- [38] M. Li, H. Yin, K. Tahara, and A. Billard, "Learning object-level impedance control for robust grasping and dexterous manipulation," in *2014 IEEE International Conference on Robotics and Automation (ICRA)*. IEEE, 2014, pp. 6784–6791.
- [39] V. R. Garate, M. Pozzi, D. Prattichizzo, N. Tsagarakis, and A. Ajoudani, "Grasp stiffness control in robotic hands through coordinated optimization of pose and joint stiffness," *IEEE Robotics and Automation Letters*, vol. 3, no. 4, pp. 3952–3959, 2018.
- [40] C. Zeng, X. Chen, N. Wang, and C. Yang, "Learning compliant robotic movements based on biomimetic motor adaptation," *Robotics and Autonomous Systems*, vol. 135, p. 103668, 2021.
- [41] E. Burdet, R. Osu, D. W. Franklin, T. E. Milner, and M. Kawato, "The central nervous system stabilizes unstable dynamics by learning optimal impedance," *Nature*, vol. 414, no. 6862, pp. 446–449, 2001.
- [42] C. Yang, G. Ganesh, S. Haddadin, S. Parusel, A. Albu-Schaeffer, and E. Burdet, "Human-like adaptation of force and impedance in stable and unstable interactions," *IEEE transactions on Robotics*, vol. 27, no. 5, pp. 918–930, 2011.
- [43] A. D. Deshpande, J. Ko, D. Fox, and Y. Matsuoka, "Control strategies for the index finger of a tendon-driven hand," *The International Journal of Robotics Research*, vol. 32, no. 1, pp. 115–128, 2013.
- [44] S. Yuan, Q. Ye, B. Stenger, S. Jain, and T.-K. Kim, "Bighand2. 2m benchmark: Hand pose dataset and state of the art analysis," in *IEEE Conference on Computer Vision and Pattern Recognition (CVPR)*, 2017.
- [45] P. Ruppel, N. Hendrich, S. Starke, and J. Zhang, "Cost functions to specify full-body motion and multi-goal manipulation tasks," in *IEEE International Conference on Robotics and Automation (ICRA)*, 2018.
- [46] C. Zeng, H. Su, Y. Li, J. Guo, and C. Yang, "An approach for robotic leaning inspired by biomimetic adaptive control," *IEEE Transactions on Industrial Informatics*, vol. 18, no. 3, pp. 1479–1488, 2021.
- [47] G. Garcia-Hernando, E. Johns, and T.-K. Kim, "Physics-based dexterous manipulations with estimated hand poses and residual reinforcement learning," *arXiv preprint arXiv:2008.03285*, 2020.



Chao Zeng received his Ph.D. degree in Pattern Recognition and Intelligent Systems from South China University of Technology (SCUT) in December 2019. Since July 2020, he is a Research Associate at the TAMS, University of Hamburg (UHH). He serves as an independent reviewer for numerous journals (e.g., TRO, TMECH, TASE, TII, TIE, RAL) and conferences (e.g., ICRA, IROS, ARM). He has also served as a Lead- or Co-Guest Editor for several journals like *Frontiers in Robotics and AI*, *Robotics and Autonomous Systems*, *Micromachines*.

His research focus is to develop learning and control approaches for robot compliant and dexterous manipulation in physical interaction task scenarios.



Shuang Li is a postdoc at the Department of Informatics, Universität Hamburg, Germany. She received her PhD (2022) in Computer Science from Universität Hamburg and her BSc (2013) and MSc (2015) in Mechanical Engineering from Anhui University of Technology. Her research interests are robotic teleoperation, dexterous manipulation and deep learning applications in robotics.



of Agile Robots AG.

Zhaopeng Chen received B.S. degree in Mechanical Engineering and Automation and M.S. degree in Mechatronic Engineering from Harbin Institute of Technology, Harbin, China, in 2005 and 2007, respectively. From 2008 to 2010, he was a joint-train Ph.D. candidate in the Institute of Robotics and Mechatronics, DLR German Aerospace Center, Oberpfaffenhofen, Germany. Since 2010, he has been with DLR German Aerospace Center in Oberpfaffenhofen, Germany, as a research scientist. Since August 2018, he has been the CEO and Co-founder



Corresponding Co-Chair of IEEE Technical Committee on Collaborative Automation for Flexible Manufacturing (CAFM), and a Fellow of British Computer Society. His research interest lies in human robot interaction and intelligent system design.

Chenguang Yang received the Ph.D. degree in control engineering from the National University of Singapore, Singapore, in 2010, and postdoctoral training in human robotics from the Imperial College London, London, U.K. He was awarded UK EPSRC UKRI Innovation Fellowship and individual EU Marie Curie International Incoming Fellowship. As the lead author, he won the IEEE Transactions on Robotics Best Paper Award (2012) and IEEE Transactions on Neural Networks and Learning Systems Outstanding Paper Award (2022). He is the



Foundation of China. He was the EIC of the Journal of Cognitive Computation and Systems, and an Associated Editors for the IEEE TRANSACTIONS ON NEURAL NETWORKS AND LEARNING SYSTEMS during 2006–2010, IEEE TRANSACTIONS ON FUZZY SYSTEMS since 2011, IEEE TRANSACTIONS ON COGNITIVE AND DEVELOPMENTAL SYSTEMS since 2018, and IEEE TRANSACTIONS ON SYSTEMS, MAN, AND CYBERNETICS: SYSTEMS since 2015.

Fuchun Sun (Fellow, IEEE) is currently a Full Professor with the Department of Computer Science and Technology, Tsinghua University, Beijing, China. His current research interests include cross-modal learning, active perception, and precise operation and teleoperation. He is a Fellow of CAA and CAAI. He was the recipient of the Excellent Doctoral Dissertation Prize of China in 2000 by MOE of China and Choon-Gang Academic Award by Korea in 2003. In 2006, he was recognized as a Distinguished Young Scholar by the Natural Science



Transregional Collaborative Research Centre SFB/TRR169 “Crossmodal Learning” and several EU robotics projects. He has been the General Chairs of the 2012 IEEE Multisensor Fusion and Integration, the 2015 IEEE/RSJ Intelligent Robots and Systems, 2018 Human Centred Robotics, etc. He is Academician of the National Academy of Engineering Sciences in Germany and the Academy of Sciences and Humanities in Hamburg Germany.

Jianwei Zhang is a Professor and the Director with Technical Aspects of Multimodal Systems Group, Department of Informatics, Universität Hamburg, Hamburg, Germany. His research interests include sensor fusion, intelligent robotics, multimodal machine learning, etc. In these areas, he has authored and co-authored about 400 journal and conference papers, technical reports, and four books.

Prof. Zhang was the recipient of multiple best paper awards. He is the Coordinator of the DFG/MSFC